# Porous metamaterials for deep sub-wavelength ultrasonic imaging

Kiran Kumar Amireddy, Krishnan Balasubramaniam, and Prabhu Rajagopal

Citation: Appl. Phys. Lett. **113**, 124102 (2018); doi: 10.1063/1.5045087
View online: https://doi.org/10.1063/1.5045087
View Table of Contents: http://aip.scitation.org/toc/apl/113/12
Published by the American Institute of Physics

# Porous metamaterials for deep sub-wavelength ultrasonic imaging

Kiran Kumar Amireddy,[a),b)] Krishnan Balasubramaniam,[b)] and Prabhu Rajagopal[b)]
*Centre for Nondestructive Evaluation and Department of Mechanical Engineering, Indian Institute of Technology Madras, Chennai 600036, Tamil Nadu, India*

(Received 16 June 2018; accepted 17 August 2018; published online 20 September 2018)

This paper reports the application of a porous medium as an aperiodic metamaterial lens for ultrasonic imaging in the context of nondestructive evaluation and non-invasive diagnostics. Experimental results are presented, demonstrating a deep sub-wavelength imaging down to 1/36th of the operating wavelength, which is the highest resolution demonstrated worldwide using bulk ultrasound. The improvement in the resolution is shown to be linked to aperiodicity overcoming the Wood anomaly, which sets limits on wave transmission by holey structured lenses. *Published by AIP Publishing.*
https://doi.org/10.1063/1.5045087

There is much interest in improving the capabilities of ultrasonic inspections, in view of the method being prone to poor resolution. However, ultrasound is non-radioactive and affordable compared to electromagnetic methods and has wide potential in healthcare and industrial diagnostics, provided that the resolution can be improved. Recent years have seen the rapid emergence of a new class of lenses based on metamaterials, offering extraordinary possibilities to control electromagnetic or acoustic waves.[1–3] Previous studies have revealed that the mechanical performance of metamaterial lenses is dependent on periodic geometrical and topographic features.[4,5] The amplification and perfect focusing by metamaterial-based lenses have potential applications in sensing, filtering,[6,7] focusing, subwavelength imaging,[8–15] cloaking,[16,17] and non-invasive medical diagnostics.[18,19] The majority of literature on metamaterial-based lenses is focused on periodic structures, with repeated unit cells of pre-designed sizes,[20] which exhibit extraordinary wave propagation due to wave scattering from periodic inhomogeneities[21] or local resonance.[22] From this perspective, a periodic holey structured metamaterial seems to be another promising alternative to control wave propagation at multi-scale frequencies. Full transmission peaks with these metamaterial lenses are due to Fabry-Perot resonances inside the features (such as holes or channels) of the periodic structures. The position and the width of the transmission peaks can be tuned by changing geometrical parameters such as the filling fraction of holes and lattice geometry of perforated plates.[23–25]

Recently, the authors reported the experimental demonstration of extraordinary transmission of wave fields through periodic holey-structures and their potential applications for deep sub-wavelength resolution and imaging (1/25th of the operating wavelength) in the ultrasonic regime for the first time worldwide.[26,27] However, one of the major drawbacks of periodic metamaterial lenses is the presence of dips in the transmission spectrum, in a phenomenon known in the literature as the "Wood anomaly."[28,29]

Recent literature, particularly in the field of acoustics, has considered lenses with quasi-periodic arrays of sub-wavelength holes and fractal geometries,[30–32] and these authors demonstrate strong resonant transmission of sound due to coherent diffraction through such structures. To identify how the geometry influences the ultrasonic transmission and to demonstrate experimentally the deep sub-wavelength resolution in the ultrasonic regime, in this paper, we discuss the use of a porous metamaterial lens. We consider a metamaterial in the form of a 3D printed porous foam, wherein the hole size varies from 2 mm to 10 mm with an average value of about 4 mm (dimensions deduced from X-ray) as shown in Fig. 1(a). The porous foam used in the experiments as a metamaterial lens was fabricated using selective laser sintering (SLS), an additive manufacturing process[33–35] at ARCI, Hyderabad, India; http://www.arci.res.in/. SLS is a 3-D printing or additive manufacturing technique which uses a high power-density laser to sinter and fuse metallic powders together. Alumina ($Al_2o_3$) powder was used in the process to make the layered foam structure (for more details about the SLS process, refer Refs. 34 and 35). This porous lens is used for the characterization of sub-wavelength spaced ($\lambda/36$) two side drilled holes (SDHs) and a through-notch of size $\lambda/36$ in an aluminum sample by ultrasonic imaging in the through-transmission mode of inspection. The performance of this porous metamaterial is compared with that of the optimized holey structured lens discussed by the authors in Refs. 26 and 27.

To demonstrate ultrasonic resolution in the deep sub-wavelength range, an aluminum sample with two side-drilled through holes of 1.5 mm diameter and separated by (outer to outer distance) 1 mm (which is about $\lambda/36$) and 2 mm ($\lambda/18$) from the top surface as shown in Fig. 1(b) is considered as the object for line scan. Immersion ultrasonic scan in the through-transmission mode was utilized for the experiments. An illustration of the experimental set-up is shown in Fig. 1(b). Commercial piezoelectric transducers [Panametrics NDT, model no. X1019, 180 kHz, and the element size 1.5 in. (38 mm), https://www.olympus-ims.com/en/ultrasonic-transducers/, Waltham, MA, USA] with a central frequency of 180 kHz are used for excitation, applied as a 3 cycle Hanning windowed tone-burst signal provided through the RITEC 4000 Pulser-Receiver (Ritec Inc., http://www.ritec-inc.com/, Warwick, USA). The aluminium sample with sub-wavelength defects (SDH or notch) was immersed in

[a)]Email: amireddykiran@gmail.com
[b)]All authors contributed equally to this work.

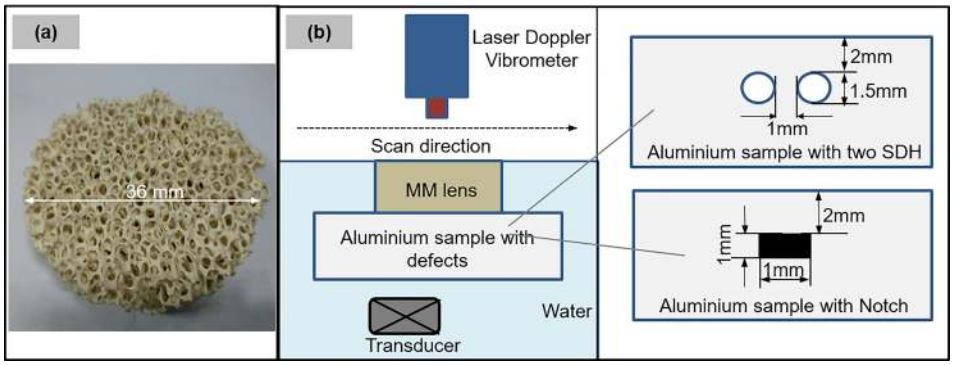


FIG. 1. (a) Photograph of the porous metamaterial foam used for experiments in this paper; (b) illustration of the experimental set-up with the details of defects considered for experiments.

water, perpendicularly in front of the transducer. The porous meta-lens is placed immediately above the sample so that the waves scattered from the defects pass through. The scattered wave fields are monitored on the surface of the porous meta-lens by using a Polytec Laser Doppler Vibrometer (LDV), consisting of an independent OFV-130 optical scanning sensor head and an OFV-551 controller (http://www.vibrometry.co.kr/OFV-552.pdf). The output from the controller is fed to a computer. A thin retroreflective tape was attached to the surface of the meta-lens at the spot illuminated by the laser point so as to enhance the optical back-scattering from the laser beam. This fiber optic head was attached to a 3-Axis scanner through a National Instruments PCI 7330 (NI Inc., http://www.ni.com/en-in.html, Austin, USA) motion controller to receive the scattered wave field in the specified scan region.

In the first case, the aluminum sample with the two sub-wavelength spaced SDH is considered as the object for line scan. The ultrasonic probe was excited at a central frequency of 180 kHz, while the scattered wave field was received by a Laser Doppler Vibrometer (LDV). The experiments are repeated for the following two cases, "without" and "with" the porous metamaterial, on the surface of the sample. After completion of the line scan, the maximum normalized amplitude variation from each A-scan (on time trace) is plotted against the measurement positions across the length of the sample. The corresponding B-scan (line scan) results for both the cases, "without the metamaterial" and "with the metamaterial," are shown in Fig. 2. The two sub-wavelength ($\lambda/36$) spaced SDH in the aluminum sample can be seen to

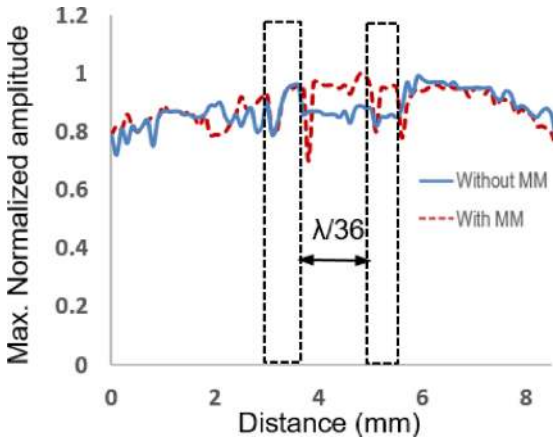


FIG. 2. Experimental results for normalized amplitude variation with the measurement position across the sample. The two rectangular boxes represent the position of the two subwavelength ($\lambda/36$) spaced side drilled holes in the aluminum sample.

be well-resolved when using the porous metamaterial as a lens. Without the meta-lens, the sub-wavelength SDH acts as perturbations and is not resolved in its line scan image.

In the next case, an aluminium sample with a through-notch (as an example of a typical canonical defect encountered in Nondestructive Evaluation-NDE applications) of length 1 mm (which is about $\lambda/36$) and located 2 mm (about $\lambda/18$) from the top surface is considered as the object for ultrasonic imaging.

The B and C-scan[33] images of the sample are obtained using the above-mentioned experimental procedure, and the corresponding results of B and C-scan images are shown in Fig. 3. The deep sub-wavelength ($\lambda/36$) notch shows up well when using the porous metamaterial as a lens. This is the highest resolution achieved as yet in the ultrasonic regime experimentally worldwide.

The image obtained by ultrasonic immersion C-scan mediated by the porous metamaterial lens was compared with that from micro X-ray Computed Tomography ($\mu$CT)[33] as shown in Fig. 3(ii-c). The crack length agrees well with the $\mu$CT image. This clearly demonstrates the resolution capacity of the porous metamaterial ultrasonic superlens.

As reported in our previous studies (see Ref. 21 for further understanding), holey-structured metamaterials act as filters for the scattered wave field and can be thought to pass high frequency components from the input to the output surface (image plane). This can be seen in the transmission spectrum of the structured metamaterial (see Ref. 26) Here, we seek to compare the transmission spectrum of the structured lens described in Ref. 26 with that of the aperiodic (porous) metamaterial discussed above. The overall dimensions of both the lenses compared are approximately the same (36 mm diameter and 24 mm length). In the structured lens, the hole size was 0.6 mm, while in the aperiodic lens, the hole size as mentioned above is much coarser.

With the holey lenses, the high frequency components scattered by sub-wavelength features get selectively amplified and are transferred to the image plane. This can be seen for example from the results in Fig. 4, showing the typical frequency content of the Transmission Ratio (TR) monitored in the experiments with the porous lens in comparison with the periodic metamaterial lens.

The full transmission peaks observed correspond to the Fabry-Perot resonance of the holes and are modulated by the interaction among holes; also, transmission dips are observed at certain frequencies corresponding to the manifestation of the Wood anomaly.[28] The Wood anomaly for the normal incidence occurs at frequencies given by[28,29]

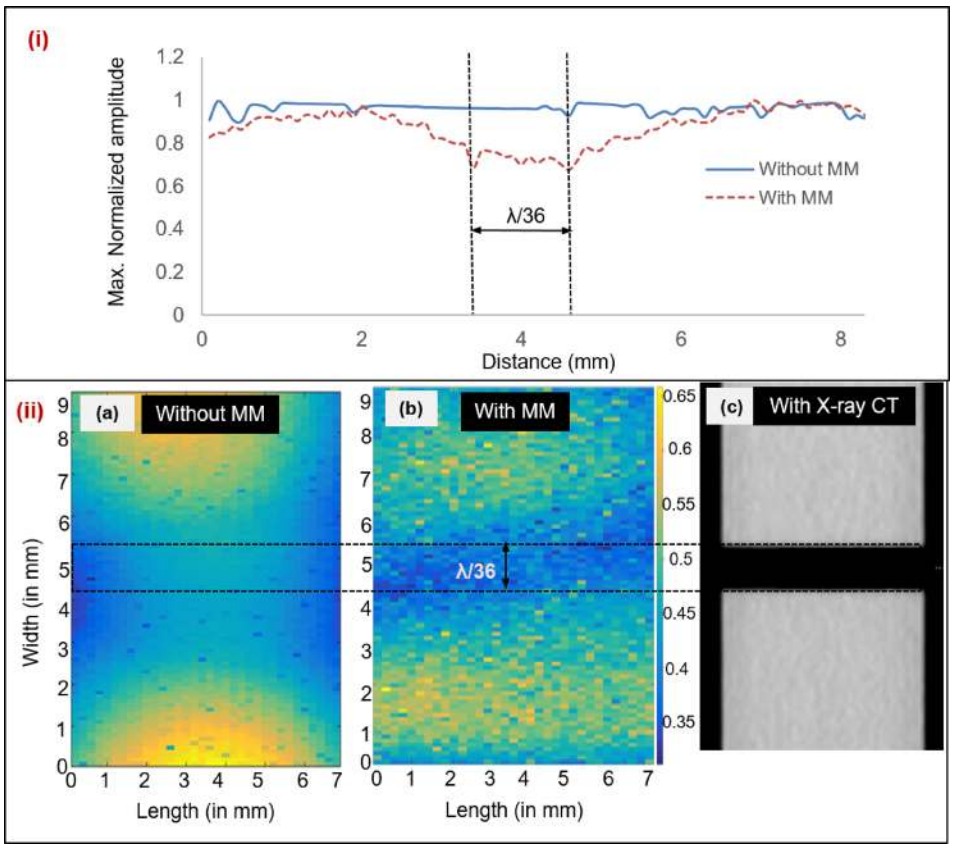


FIG. 3. Experimental results for ultrasonic (i) B-scan (line Scan); (ii) C-scan image of through-notch in the aluminium sample: (a) without and (b) with the metamaterial lens: the dotted rectangular box indicates the actual positions of the notch in the sample; (c) presents an image of the same defect as obtained by X-ray computed tomography.

$$\frac{2\pi f}{c} = \sqrt{\left(\frac{2\pi m}{p}\right)^2 + \left(\frac{2\pi n}{p}\right)^2}, \tag{1}$$

where $p$ is the hole periodicity, $c$ is the velocity of the ultrasound in water, and $m$ and $n$ are higher order resonance harmonics.

(or)

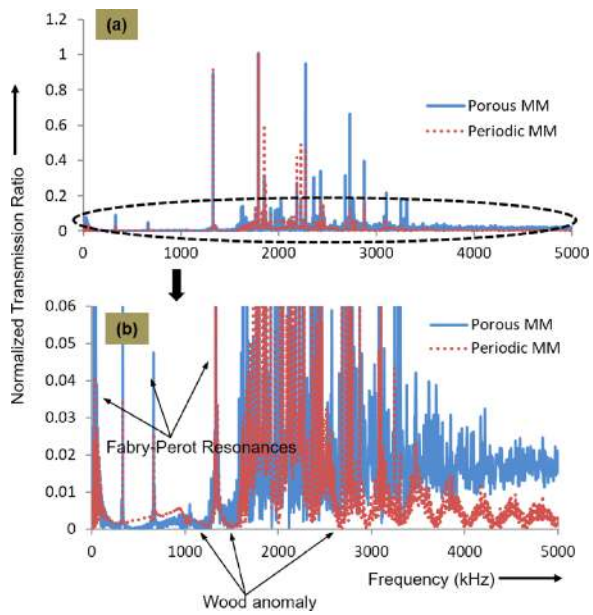


FIG. 4. Experimental results for the Transmission Ratio (TR) of Periodic and Porous metamaterial lenses. (a) Comparison of TR for both meta-lenses; (b) TR in the zoomed region for identification of Fabry-Perot resonances and Wood anomalies.

$$f = \frac{c}{p}\left(\sqrt{m^2 + n^2}\right). \tag{2}$$

The velocity of ultrasound in water ($c$) is 1500 m/s, and for the optimized periodic holey-structured meta-lens, the period ($p$) is 1.2 mm (which is used for deep sub-wavelength ultrasonic imaging in Ref. 26) Using Eq. (2), the frequency corresponding to the Wood anomaly considering only Fabry-Perot resonance and neglecting all higher order harmonics (i.e., $m = 1$ *and* $n = 0$) is ~1250 Hz. The frequency corresponding to the Wood anomaly considering Fabry-Perot resonance and 1st order harmonics (i.e., $m = 1$ *and* $n = 1$) is ~1767.76 Hz. These values are in good agreement with the TR obtained for the periodic metamaterial lens with experiments, as shown in Fig. 4(b).

If the hole size and period change, the frequencies corresponding to the Wood anomaly also change. The kind of porous metamaterial lens used in the study may be thought to consist of layers with varying periods and hole sizes, for example, as seen in the X-ray computed tomography image, shown in Fig. 5.

In order to gain more insight into the wave propagation through unstructured layered media and understand the phenomenon of Wood anomaly, 2-D simulations were implemented in a commercially available Finite Element (FE) package.[36] A 2-D FE model was created with dimensions $300 \times 250\,\text{mm}^2$, chosen to avoid reflections from the model boundaries. The model renders the porous metamaterial in the form of layers each of which has holes (as shown in Fig. 6) with randomly assigned sizes (in the range of 2–10 mm, the same range as used in the experiments). $m$ layers of thickness $n$ were considered (where $m$ varies from 1 to 9) such that the

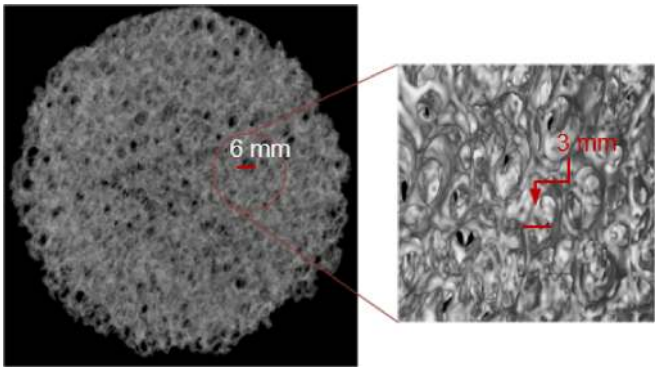


FIG. 5. X-ray computed tomography image of the porous metamaterial lens; the inset shows the zoomed view of the encircled region.

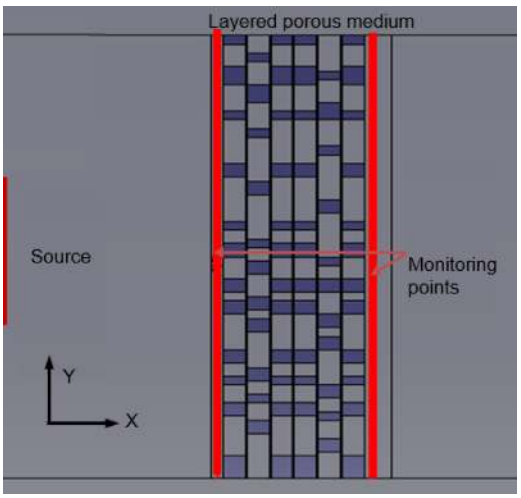


FIG. 6. Schematic of the layered porous metamaterial lens modeled in FE simulations.

total thickness of 24 mm approximates the thickness of the experimental metamaterial. A 4-noded quadrilateral mesh with a seed size of 0.1 mm ($\lambda/83$) was used. Water (acoustic medium) properties were assigned for the entire model with density $\rho$ of 1000 kg/m$^3$ and Bulk Modulus K 2.2 GPa. The 2-D holey structured metamaterial with random periodicity is realized by setting rigid (pressure is zero) boundary conditions on the selected nodal lines. Ultrasonic waves are generated in the model by exciting the left boundary of the model sample in the "x" direction with 3 cycle Hanning windowed tone burst signals centered at 180 kHz. Ultrasonic wave propagation in the sample is then simulated using the explicit FE algorithm provided by the commercial package.[36] Analysis was run for a total time period of 110 $\mu$s which is sufficient for longitudinal waves to reach the right end of the whole model. Nodes along a vertical line at a fixed distance from the meta-lens were chosen for monitoring the waves transmitted by the meta-lens.

After obtaining the A-scans at the monitoring positions, the transmission ratio (TR) of the layered meta-lens was calculated and the same is compared with experimentally obtained TR. A number of studies were performed, by varying the values of $m$ and $n$, and an optimal good agreement with experiments was observed for $m = 6$, $n = 4$. The TR results obtained using such a 6-layered porous metamaterial compared with those obtained from experiments are shown in Fig. 7. We find a broadly good agreement between the simulations and experiments, whereby the simulated layered meta-lens may then be taken to represent the experimental meta-lens in an approximation. Moreover, such an agreement, at least qualitatively, also brings out how the layered nature of the meta-lens underpins its transmission spectrum.

In the next case, the same model was used for obtaining the TR for each successive layer and compared with the overall TR of the layered metamaterial lens. The corresponding results with the approximately identified Wood anomaly for each sub-layer case are shown in Fig. 8. The frequency corresponding to the Wood anomaly in each layer is different, for layer 1, it is around 100 kHz as indicated with WAL1 in Fig. 8. The same for layer1 + layer 2 is in the range of 200–350 kHz, indicated as WAL2, and for layer1 + layer 2 + layer 3, it is around 420 kHz, indicated as WAL3 in Fig. 8. No definitive Wood anomaly was observed for the combinations of layers 1–4, 1–5, and 1–6. Hence, it is clear that the Wood anomaly in one layer is overcome by the other layer and the overall TR is the cumulative response of individual layers.

In the porous metamaterial with a random hole size and periodicity, the Wood anomaly occurs differently in each layer and is significantly diminished cumulatively. Hence, the Wood anomaly may not be observed in the transmission ratio (TR) of such a porous metamaterial lens as shown in

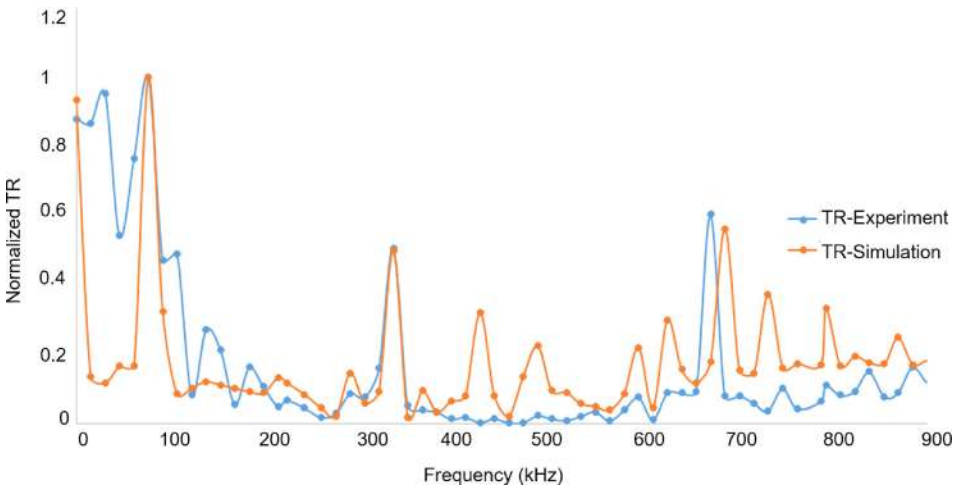


FIG. 7. Comparison of Transmission Ratio spectra obtained from experiments with the results from a simulated 6-layered porous metamaterial.

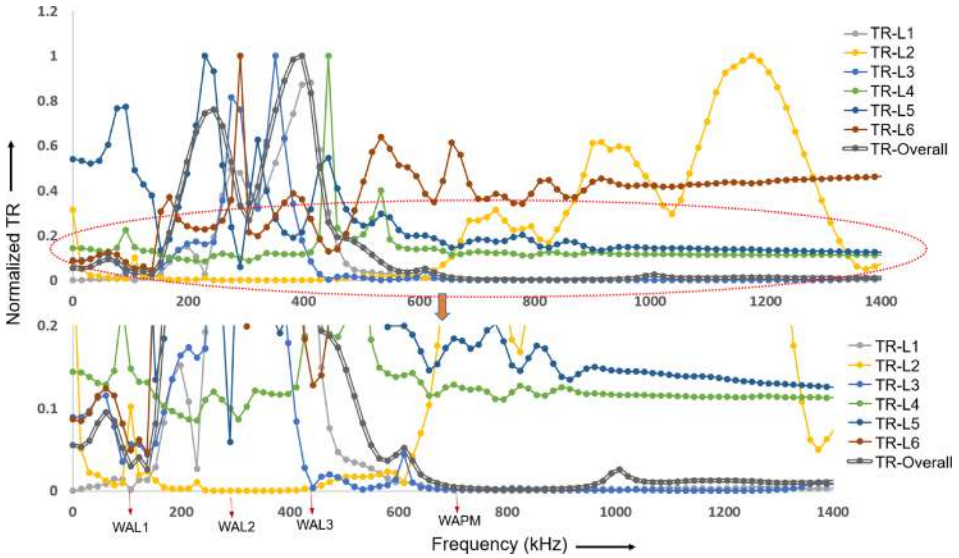


FIG. 8. FE simulated results showing the Transmission Ratio (TR) of the 6 layered metamaterial in comparison with the single layered metamaterial. The inset shows the zoomed region for identification of Wood anomalies in different layers (where WAL1, WAL2, and WAL3 are the Wood anomalies in the 1st layer, the 2nd layer, and the 3rd layer, respectively, and WAPM is the overall Wood anomaly of the porous medium).

Figs. 4(b) and 8. Thus, the higher order frequency (evanescent field) components are more effectively transferred to the image plane with this porous lens, and hence, with this, the resolution is further improved compared to the periodic metamaterial lens.

This paper demonstrated the applications of the porous metamaterial lens for deep sub-wavelength ultrasonic imaging. The meta-lens improves the resolution of imaging down to a feature size of $\lambda/36$ (where $\lambda$ is the operating wavelength) by amplifying the evanescent wave fields through the Fabry-Perot resonance phenomenon. An advantage of this approach is that the phenomenon of Wood anomaly can be avoided, and hence, all high frequency (evanescent) components can reach the image plane through the porous meta-lens.

The porous metamaterial lens used in the experiments was prepared with the ceramic (alumina) material by the selective laser sintering process at ARCI, Hyderabad, India; http://www.arci.res.in/.

The authors declare no competing financial interests.

[1]D. Schurig, J. J. Mock, B. J. Justice, S. A. Cummer, J. B. Pendry, A. F. Starr, and D. R. Smith, Science **314**(5801), 977–980 (2006).
[2]F. Wen, Y. Bing, W. Zengbo, and W. Limin, Sci. Adv. **2**(8), e1600901 (2016).
[3]J. Neu, B. Krolla, O. Paul, B. Reinhard, R. Beigang, and M. Rahm, Opt. Express **18**(26), 27748–27757 (2010).
[4]S. Cranford, A. Tarakanova, N. Pugno, and M. N. Buehler, Nature **482**, 72–76 (2012).
[5]R. Zaera, A. Soler, and J. Teus, J. R. Soc. Interface **11**, 20140484 (2014).
[6]K. Song, S.-H. Lee, K. Kim, S. Hur, and J. Kim, Sci. Rep. **4**, 4165 (2014).
[7]R. Martinez-Sala, J. Sancho, J. V. Sanchez, V. Gomez, J. Llinares, and F. Meseguer, Nature **378**, 241 (1995).
[8]J. Zhu, J. Christensen, J. Jung, L. Martin-Moreno, X. Yin, L. Fok, X. Zhang, and F. J. Garcia-Vidal, Nat. Phys. **7**, 52–55 (2011).
[9]K. Deng, Y. Ding, Z. He, H. Zhao, J. Shi, and Z. Liu, J. Appl. Phys. **105**, 124909 (2009).
[10]S. A. Cummer, J. Christensen, and A. Andrea, Nat. Rev. Mater. **1**, 16001 (2016).
[11]Y. Cheng, C. Zhou, Q. Wei, D. Wu, and X. Liu, Appl. Phys. Lett. **103**, 224104 (2013).
[12]Y. Gu, Y. Cheng, and X. Liu, Appl. Phys. Lett. **107**, 133503 (2015).
[13]J. Zhang, Y. Cheng, and X. Liu, Appl. Phys. Lett. **110**, 233502 (2017).
[14]J. Christensen and F. J. Garcia de Abajo, Phys. Rev. Lett. **108**, 124301 (2012).
[15]Y. Cheng, C. Zhou, B. G. Yuan, D. J. Wu, Q. Wei, and X. J. Liu, Nat. Mater. **14**, 1013–1019 (2015).
[16]N. Fang, D. Xi, J. Xu, M. Ambati, W. Srituravanich, C. Sun, and X. Zhang, Nat. Mater. **5**, 452–456 (2006).
[17]S. Zhang, C. Xia, and N. Fang, Phys. Rev. Lett. **106**, 024301 (2011).
[18]B. Thierry, S. Faghihi, L. Torab, G. Pike, and M. Tabrizian, Adv. Mater. **17**, 826 (2005).
[19]C. M. Soukoulis and M. Wegener, Nat. Photonics **5**, 523–530 (2011).
[20]Y. J. Tsai, S. Larouche, T. Tyler, G. Lipworth, N. M. Jokerst, and D. R. Smith, Opt. Express **19**(24), 24411–24423 (2011).
[21]L. Brillouin, *Wave Propagation in Periodic Structures* (McGraw-Hill Book Company, 1946).
[22]Z. Liu, X. Zhang, Y. Mao, Y. Y. Zhu, Z. Yang, C. T. Chan, and P. Z. Sheng, Science **289**, 1734–1736 (2000).
[23]H. Estrada, P. Candelas, A. Uris, F. Belmar, F. Meseguer, and F. J. Garcia de Abajo, Appl. Phys. Lett. **93**, 011907 (2008).
[24]H. Estrada, P. Candelas, A. Uris, F. Belmar, F. J. Garcia de Abajo, and F. Meseguer, Appl. Phys. Lett. **95**, 051906 (2009).
[25]H. Estrada, P. Candelas, A. Uris, F. Belmar, F. Meseguer, and F. J. Garcia de Abajo, Wave Motion **48**, 235–242 (2011).
[26]K. K. Amireddy, K. Balasubramaniam, and P. Rajagopal, Sci. Rep. **7**, 7777 (2017).
[27]K. K. Amireddy, K. Balasubramaniam, and P. Rajagopal, Appl. Phys. Lett. **108**, 224101 (2016).
[28]H. Estrada, V. Gomez-Lozano, A. Uris, P. Candelas, F. Belmar, and F. J. Meseguer, Ultrasonics **52**, 412–416 (2012).
[29]A. Uris, V. Gomez-Lozano, P. Candelas, and F. Belmar, Acta Acust. Acust. **100**, 595–603 (2014).
[30]R. Hao, H. Jia, Y. Ye, F. Liu, C. Qiu, M. Ke, and Z. Liu, Eur. Phys. Lett. **92**, 24006 (2010).
[31]H. Hao, C. Qiu, Y. Hu, K. Tang, and Z. Liu, Phys. Lett. A **375**, 4081–4084 (2011).
[32]B. B. Mandenelbrot, *The Fractal Geometry of Nature* (W.H. Freeman & Co., New York, 1983).
[33]K. Raguvarun, K. Balasubramaniam, P. Rajagopal, S. Palanisamy, R. Nagarajah, N. Hoye, D. Curiri, and A. Kapoor, in *41st Annual Review of Progress in Quantitative NDE* (American Institute of Physics, 2015), Vol. 1650, pp. 146–155.
[34]M. Agarwala, D. Bourell, J. Beaman, H. Marcus, and J. Barlow, Rapid Prototyping J. **1**(1), 26–36 (1995).
[35]See www.xometry.com for Direct Metal Laser Sintering – Xometry; accessed 18 January 2018.
[36]See http://www.3ds.com/products/simulia/portfolio/abaqus/abaqus-portfoliofor ABAQUS. Analysis User's Manual. Version 6.10-1; accessed 28 June 2018.